

AD-A074 907

PURDUE UNIV LAFAYETTE IN TURNER LAB FOR ELECTROCERAMICS F/G 9/1
THE EFFECTS OF SUBSTRATE COMPOSITION ON THICK FILM CIRCUIT RELI--ETC(U)
AUG 79 R W VEST N00019-79-C-0240

UNCLASSIFIED

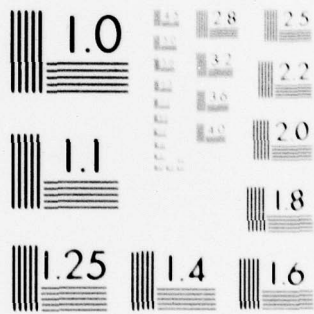
NL

| OF |

AD
A074907



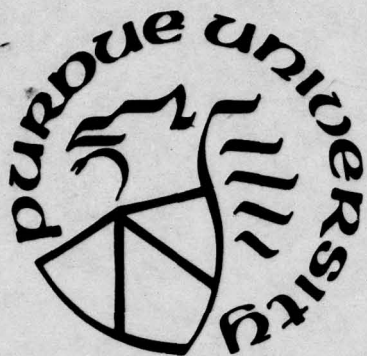
END
DATE
FILMED
11-79
DDC



MICROCOPY RESOLUTION TEST CHART
NATIONAL BUREAU OF STANDARDS-1963-A

~~TOP SECRET~~

APPROVED FOR PUBLIC RELEASE
DISTRIBUTION UNLIMITED



LEVEL II

10

PURDUE UNIVERSITY
West Lafayette, Indiana

ADA074907



DDC FILE COPY

SCHOOL OF MATERIALS ENGINEERING

DISTRIBUTION STATEMENT A
Approved for public release
Distribution Unlimited

DDC
RECEIVED
OCT 11 1979

79 10 10 016

12

THE EFFECTS OF SUBSTRATE COMPOSITION
ON THICK FILM CIRCUIT RELIABILITY

R. W. Vest

31 August 1979

Quarterly Report No. 2

For the period 5/1/79-4/31/79

Contract No. N0019-79-C-0240

Prepared for

NAVAL AIR SYSTEMS COMMAND

DDC
RECEIVED
OCT 11 1979
A

Accession For	
NTIS GRA&I	<input checked="" type="checkbox"/>
DDC TAB	<input type="checkbox"/>
Unannounced	<input type="checkbox"/>
Justification	
N0019-79-C-0240	
By _____	
Distribution/	
Availability Codes	
Dist.	Avail and/or special
A	

FOREWORD

Research described in this report constitutes the second three months of effort under Contract No. N0019-79-C-0240 with the Naval Air Systems Command, Department of the Navy, under the technical cognizance of James Willis. The research was conducted in the Turner Laboratory for Electroceramics, School of Materials Engineering and School of Electrical Engineering, Purdue University, West Lafayette, Indiana 47907, under the direction of Professor R. W. Vest. Contributing to the project were Messrs. J. M. Himelick, P. Palanisamy, and R. L. Reed.

D D C
OCT 11 1979
A

SECURITY CLASSIFICATION OF THIS PAGE (When Data Entered)

REPORT DOCUMENTATION PAGE		READ INSTRUCTIONS BEFORE COMPLETING FORM
1. REPORT NUMBER 2	2. GOVT ACCESSION NO.	3. RECIPIENT'S CATALOG NUMBER
4. TITLE (and Subtitle) 6 THE EFFECTS OF SUBSTRATE COMPOSITION ON THICK FILM CIRCUIT RELIABILITY.		5. TYPE OF REPORT & PERIOD COVERED 5/1/79-7/31/79
		6. PERFORMING ORG. REPORT NUMBER
7. AUTHOR(s) 10 R. W. Vest	9. PERFORMING ORGANIZATION NAME AND ADDRESS PURDUE RESEARCH FOUNDATION, PURDUE UNIVERSITY, West Lafayette, Indiana 47907	8. CONTRACT OR GRANT NUMBER(s) 15 NO 19-79-C-0240
11. CONTROLLING OFFICE NAME AND ADDRESS NAVAL AIR SYSTEMS COMMAND, AIR 310B Washington, D.C. 20361		10. PROGRAM ELEMENT, PROJECT, TASK AREA & WORK UNIT NUMBERS 12 48
14. MONITORING AGENCY NAME & ADDRESS (if different from Controlling Office)	12. REPORT DATE 31 August 1979	13. NUMBER OF PAGES 42
		15. SECURITY CLASS. (of this report) Unclassified
16. DISTRIBUTION STATEMENT (of this Report) APPROVED FOR PUBLIC RELEASE DISTRIBUTION UNLIMITED	13. NUMBER OF PAGES 42	16. DECLASSIFICATION/DOWNGRADING SCHEDULE N/A
		17. DISTRIBUTION STATEMENT (of the abstract entered in Block 20, if different from Report) 9 Quarterly rept. no. 2, 1 May - 31 Jul 79.
18. SUPPLEMENTARY NOTES		
19. KEY WORDS (Continue on reverse side if necessary and identify by block number) Thick Film Resistors Temperature Coefficient Resistivity Ceramic Substrates Electronic Glass Electrical Resistivity Glass Sintering		
20. ABSTRACT (Continue on reverse side if necessary and identify by block number) Measurements of the high temperature viscosities and surface tensions of thick film glasses as a function of temperature and amount of AlSiMag 614 substrate dissolved in the glasses were completed. Both glass properties were observed to increase with increasing amount of dissolved substrate at all temperatures. The non-sintered contacts occurring in the RuO ₂ networks of thick film resistors were modeled using MIM devices. The		

DD FORM 1 JAN 73 1473

EDITION OF 1 NOV 68 IS OBSOLETE
S/N 0102-014-6601

SECURITY CLASSIFICATION OF THIS PAGE (When Data Entered)

410 421 mit

↙ Abstract continued

dominant charge transport mechanism for glass films >7nm at room temperature and above was Schottky emission; for thinner films and/or lower temperatures, quantum mechanical tunneling becomes important ↘

TABLE OF CONTENTS

	Page
1. INTRODUCTION	1
2. MICROSTRUCTURE DEVELOPMENT	4
3. METAL-SIMULATOR-METAL STUDY	10
3.1 Fabrication	11
3.2 Anneal Experiments	14
3.3 AC Conductivity and Dissipation Factor	15
3.4 Dielectric Constant and Dielectric Breakdown	21
3.5 DC Experiments	23
4. FUTURE WORK	40
5. REFERENCES	41
6. STATEMENT OF ESTIMATED COSTS	42

1. INTRODUCTION

The print and fire processing of thick film circuits ensures that there always will be some degree of chemical interaction between the film and the substrate, because all common substrate materials are soluble to some degree in the glasses used in thick film inks. This interaction is primarily responsible for the development of adhesion between the thick film and the substrate, but it also leads to changes in the composition of the glass with the net result that the physical properties of the glass will change. These changes in physical properties of the glass will result in modified kinetics for the various microstructure development processes and all electrical properties of the resistors are related to the microstructure. The goal of this research program is to develop a sufficient level of understanding of the phenomena involved so that appropriate models can be developed. These models should lead to the writing of specifications for impurity limits and additive ranges for substrates, and to recommendations concerning glass composition and processing conditions.

Previously reported studies [1-4] under this program have established the magnitude of the effects resulting from chemical interaction between a thick film resistor and a ceramic substrate, and have determined the specific influence on important properties of the resistor glass. The rates of dissolution of two substrates, 96 percent Al_2O_3 (AlSiMag 614) and 99.5 percent Al_2O_3 (AlSiMag 772), in two lead borosilicate glasses (63 w/o PbO -25 w/o B_2O_3 -12 w/o SiO_2 and 70 w/o PbO -20 w/o B_2O_3 -10 w/o SiO_2) were measured at

various temperatures. The rate limiting steps for each substrate-glass system were determined in all appropriate temperature ranges, and analytical equations were developed to predict the substrate recession as a function of time and temperature for thick film resistors. The saturation solubility of AlSiMag 614 (96 percent Al_2O_3) substrates in 63-25-12 glass was determined as a function of temperature, and these results were combined with the dissolution rate studies in order to test various kinetic models. Studies of the kinetics of initial stage sintering of glass particles were conducted in order to determine the ratio of surface tension to viscosity for the two standard glasses, and the standard glasses with additions of substrate ingredients. Both the magnitude and the activation energies of this ratio were found to be significantly different for the glasses, confirming the extreme sensitivity of this parameter to small changes in glass composition. The viscosity of the 63-25-12 glass was measured as a function of amount of dissolved AlSiMag 614 substrate from the softening point to the annealing point. The isothermal viscosity was found to increase by a factor of 20 with 10 w/o dissolved substrate relative to the standard lead borosilicate glass. The affects of the minor constituents (4 percent) in the AlSiMag 614 substrate composition on viscosity and surface tension of the glasses was determined to be small. The ripening kinetics of RuO_2 particles in all glass compositions were in agreement with a phase boundary reaction rate limiting step, and the rate constant was observed to decrease by a factor of 4 when the amount

of dissolved substrate reached 10 w/o. The sheet resistance, temperature dependence of resistance, and the current noise were measured for thick film resistors as a function of the amount of substrate dissolved in the resistor for various firing temperatures at constant firing time, and for various firing times at 800°C. Large variations in these three properties were observed, and the changes were qualitatively correlated with changes in viscosity of the glass. The microstructure development and charge transport models used to correlate the results indicated a retardation of microstructure development in the resistors as the amount of dissolved substrate increased which led to changing proportions of sintered and nonsintered contacts in the RuO_2 networks within the body of the resistor.

2. MICROSTRUCTURE DEVELOPMENT

2.1 High Temperature Viscosity of Glasses

The high temperature viscosity of glasses as a function of the amount of the dissolved substrate was determined by the sphere method as outlined in the previous report [4]. The viscosity results for the various glass compositions are presented as a function of temperature in Figure 1. The excellent agreement between the viscosity of NBS 711 glass determined in this work and that recommended by the National Bureau of Standards is also shown in Figure 1. The isothermal viscosity increases with increases in substrate content of the glass.

The fact that the temperature dependence of viscosity cannot be adequately represented by a simple Arrhenius equation is demonstrated by the curvature of the lines in Figure 2. A better fit was obtained using an empirical equation proposed by Fulcher [5],

$$\log \eta = A + B/(T-T_0) \quad (1)$$

in which

η = viscosity

T = temperature

$A, B,$ and T_0 are empirical constants

The results of these calculation are given in Table 1, and the fit is excellent; the coefficients of determination (r^2) are greater than .9998 and the standard deviations (σ) are low.

The viscosity curve for the glass with 8 w/o dissolved alumina falls between those for the 6 w/o substrate glasses, indicating that the minor constituents (4 w/o) in the AlSiMag 614 substrate

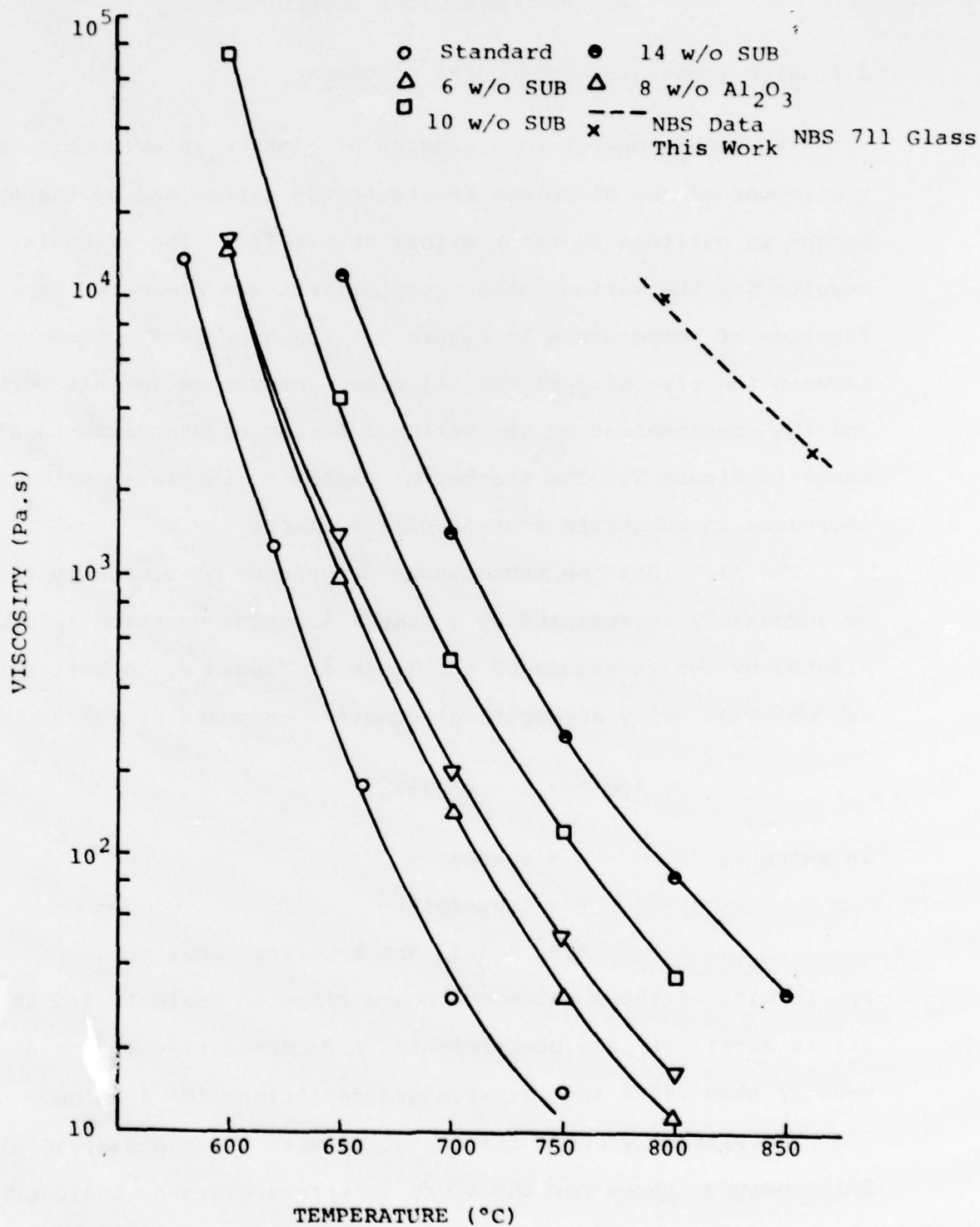


Figure 1. Viscosity of Standard Glass (63 w/o PbO-25 w/o B₂O₃-12 w/o SiO₂) with Various Amounts of Dissolved AlSiMag 614 Substrate

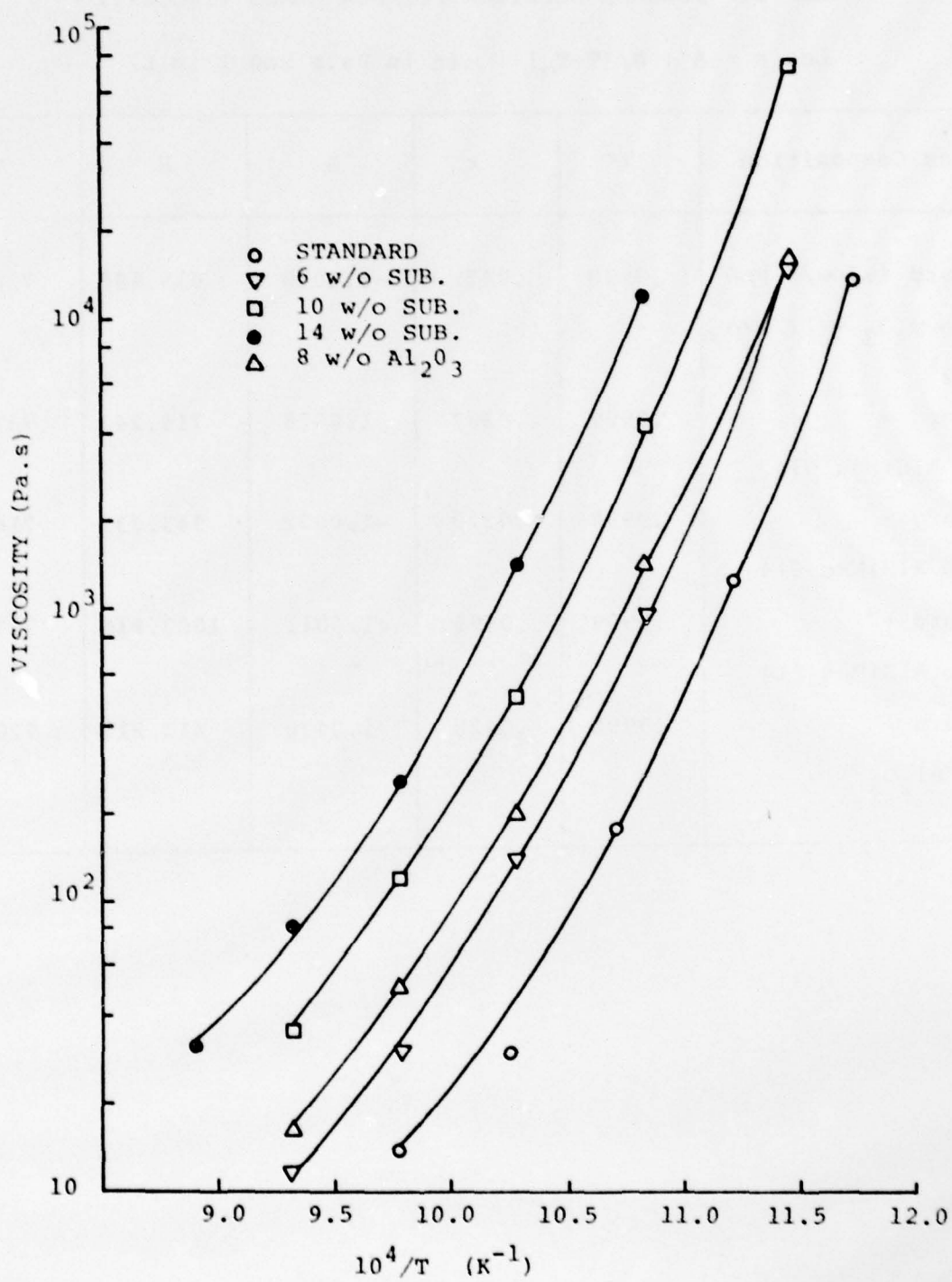


Figure 2. Arhenius Plot of Viscosity Data from Figure 1

Table 1. FULCHER EQUATION FIT FOR GLASS VISCOSITY

$$\text{Log } \eta = A + B/(T-T_0) \quad (\eta \text{ in Pa.s and } T \text{ in K})$$

Glass Composition	r^2	r	A	B	T_0
Standard (63 w/o PbO 25 w/o B ₂ O ₃ - 12 w/o SiO ₂)	.9998	.0431	-1.0010	615.695	736.69
Standard + 6 w/o AlSiMag 614	.9999	.0387	-1.0026	716.243	737.78
Standard + 10 w/o AlSiMag 614	.9999	.0329	-1.0022	945.335	714.44
Standard + 14 w/o AlSiMag 614	.9999	.0195	-1.0011	1003.810	727.15
Standard + 8 w/o Al ₂ O ₃	.9998	.0428	-1.0430	813.211	720.63

do not have a significant effect on the high temperature viscosity of these glasses.

2.2 Surface Tension of Glasses

The experimental techniques and some preliminary results of high temperature surface tension measurements on glasses were presented in the previous report [4]. The complete results of this study are presented in Figure 3. The addition of substrate or alumina increases the isothermal surface tension of the base glass. The surface tension-temperature curves for the substrate or alumina doped glasses show a minimum near 800°C, whereas the surface tension of the standard glass continues to decrease with increasing temperature. The surface tension values for the 8 w/o alumina glass are the same, within experimental error, as those of the 10 w/o substrate glass. The minor constituents (4 w/o) in the substrate tend to reduce the effect of Al_2O_3 in increasing the surface tension of the standard glass.

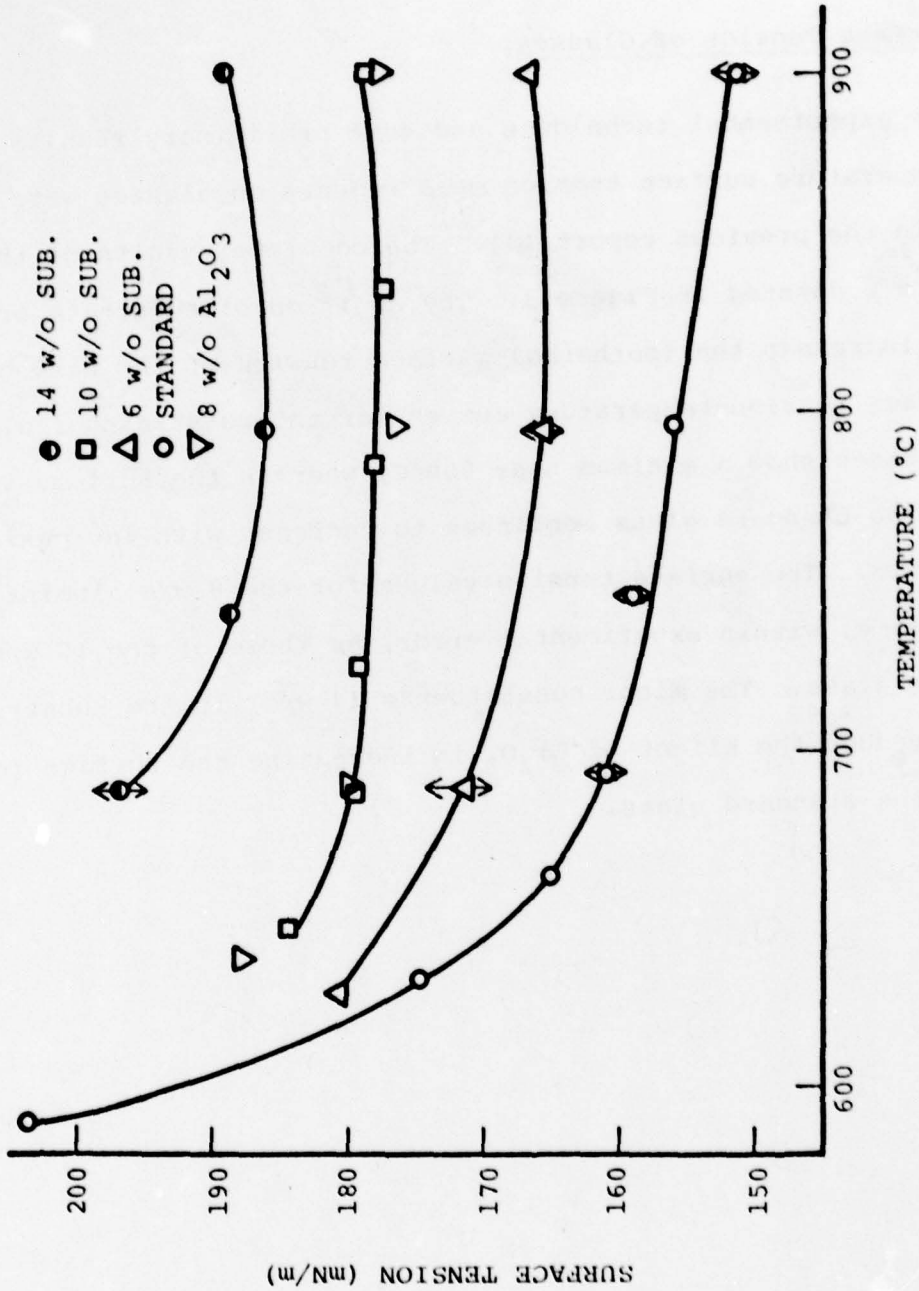


Figure 3. Surface Tension of Standard Glass (63 w/o PbO - 25 w/o B₂O₃ - 12 w/o SiO₂) with Various Amounts of Dissolved AlSiMag 614 Substrate

3. METAL - INSULATOR - METAL STUDY

Thick film resistors contain multi-stranded networks of conducting particles. A large number of these particles will be joined by sintered necks, but a significant fraction will be separated by a thin layer of glass, thus forming non-sintered contacts. As a result of the firing process, the non-sintered contacts will have a continuous range of glass barrier thicknesses, from a few atomic layers to several thousand atomic layers. In addition, there could also be compositional variations and impurities present in the glass films due to substrate dissolution during firing. Because of the variance of the film thickness and composition, electrical conduction through the non-sintered contact may occur by more than one mechanism. For example, a tunneling mechanism may be important for very thin films, but as the tunneling resistance increases exponentially with film thickness, another mechanism such as Schottky or Frenkel-Poole emission may dominate.

In order to develop a complete model for charge transport it is necessary to be able to predict the conduction through the non-sintered contacts as a function of film thickness and glass composition. The achievement of this goal was complicated by the fact that there are no experimental techniques available to measure the conduction mechanisms in these "micro" contacts as they appear in thick film resistors. However, the geometry of a non-sintered contact is similar to a parallel plate capacitor, where the conducting particles represent the metal plates, and the glass layer corresponds to the dielectric. Thus, the MIM structure lends itself

very well to the study of conduction in thin films. Ideally, the metal electrodes of the MIM device should be the same composition as the conducting phase in the thick film resistors (RuO_2 in our case). This ideal geometry could not be realized because RuO_2 cannot be deposited as a coherent film by any known means, and gold electrodes were substituted. The principal effect of changing electrode materials will be the differences in work functions, which enters into several charge transport mechanisms.

3.1 Fabrication

The glass films for the MIM devices were deposited by rf sputtering from a specially prepared target. Two glass compositions were used in the MIM devices: the standard glass (63 w/o PbO -25 w/o B_2O_3 -12 w/o SiO_2), and the standard glass with 10 w/o AlSiMag 614 substrate dissolved in it. The targets were made by melting the glass in a platinum crucible followed by casting in a stainless steel mold. The targets were examined for cracks, devitrification, or impurities, and then annealed at 450°C for a minimum of two hours to relieve any strains which may have been introduced from the casting operation. The final step in target preparation was to bond the glass with a conducting epoxy cement to an aluminum blank which could be mounted in the sputtering system.

Because of the extremely thin films (typically < 35 nm) that were sputtered, substrate preparation was a very critical step in the fabrication of the MIM devices. Polished, single-crystal silicon wafers (commonly used in integrated circuit fabrication) were

chosen for the substrate material. Following an initial cleaning procedure, the wafers were oxidized at 1100°C for one hour. The resulting 110nm SiO₂ layer was needed to isolate the lower electrode of the MIM structure from the silicon, both electrically and physically. Following the oxidation step, the wafers were metallized on one side by vacuum evaporating a layer of chromium (~ 50nm) immediately followed by a layer of gold (~ 50-100 nm) to serve as the bottom electrode. The chromium interlayer was used to aid adhesion between the SiO₂ and gold. The wafers were placed in an rf sputtering unit approximately 5 cm from the target with a movable shutter positioned between the two. To initiate a sputtering run, the vacuum chamber was backfilled to 1.6-2.1 Pa with a 50:50 mixture of Ar and O₂, and the plasma ignited. After the plasma had been on long enough to insure that a constant composition was being sputtered from the glass target, the shutter was opened for the length of time required to produce the desired film thickness.

Employing the same vacuum system and procedures used for the Cr-Au bottom electrodes, gold counter-electrodes were deposited in a dot pattern on the glass film by evaporating through a metal mask. Chromium was not used for the counter-electrodes because the structure desired was Au-glass-Au, not Au-glass-Cr, and the chromium was not needed for adhesion to the glass. Following metallization, the wafers were scribed with a diamond stylus into chips approximately 0.5 cm X 0.5 cm and each chip was etched to remove the glass from the edges, thus allowing the bottom electrode

to be exposed. Following the etching procedure, devices were annealed at 440°C for 15 minutes in an oxygen atmosphere; the experiments used to determine the optimum anneal time and temperature will be discussed in Section 3.2. Samples that were to be temperature cycled were mounted on 8-pin, gold coated headers using a small quantity of conducting epoxy.

The sputtered glass thickness was measured with an optical interference instrument using monochromatic sodium light ($\lambda = 589\text{nm}$). The film thickness, s , is determined by the amount of offset in the interference lines relative to the separation of adjacent lines. The error in measuring very thin films ($< 30\text{nm}$) can be quite large; however, this proved to be the only available way of measuring s . Profilometry techniques were unsatisfactory due to the scratching of the soft glass by the stylus, interferometer measurements require a more complete understanding of the refractive index to be useful, and capacitance measurements require a knowledge of the variation of the dielectric constant with thickness.

It was found that there was a good correlation between sputtering time and film thickness, especially for the thicker films ($> 50\text{nm}$). Holding the power and pressure constant, a constant sputtering rate could be achieved, and the sputtering time required for a desired thickness was easily calculated. However, as the sputtering times were shortened, the sputtering rate varied due to fluctuations in the rf power during the initial tuning and to a change in the sputtering efficiency resulting from initial charging of the target and substrate.

In addition to the MIM devices, bulk glass capacitors were made from the two glass compositions, standard and standard with 10 w/o substrate added. The glass was melted in a platinum crucible at 900°C and poured into a heated stainless steel mold. The mold was allowed to cool to room temperature, and the casting examined for cracks, bubbles, or devitrification. Good quality glass blanks were then annealed at 450°C for a minimum of two hours in air. Cylinders, 16.3mm and 7.5mm diameter, were cut from the blank using a diamond core drill, and then sliced into 0.3 to 0.8mm thick sections using a slow speed diamond saw. The samples were then polished and provided with evaporated gold electrodes.

3.2 Anneal Experiments

After the gold counter electrode deposition, the films were annealed to reduce some of the damage done during the sputtering operation. Sputtering is a high energy process which can induce stresses in the film due to the impact of accelerated ionized particles, and some of the constituent oxides in the target may dissociate during deposition even though maintaining a partial pressure of oxygen during sputtering will reoxidize a portion of these. In addition, the density of the film may be lower than that of the bulk glass because of the random orientation of depositing glass units.

Annealing times and temperatures were selected with reference to the results of the studies of viscosity as a function of temperature and composition presented in Section 2.1. The devices were

annealed by placing the chips in a fused quartz boat, and heating in a fused quartz-lined furnace at 380°C to 440°C under a constant oxygen flow. The anneal times investigated at 380°C were 30 minutes, 1, 2, 4, 6, and 8 hour accumulative, that is, a one hour anneal was the initial 30 minutes plus a second 30 minute anneal after electrical testing.

Devices under test were placed on a vacuum chuck in a light-tight, grounded metal box. A micropositioner with a spring-loaded probe was used to make contact to the lower electrode at a corner of the sample where the glass had previously been etched away. A second micropositioner with a spring-loaded probe was used to make contact to the top electrodes of the devices. The complex admittance of each device was measured from 100 Hz to 100 kHz with a transformer ratio arm bridge.

The results of the anneal experiments were presented in an earlier report [3]. Overall, there was an improved electrical behavior for annealed devices over unannealed ones. The capacitance changed very little, but the conductivity and the dissipation factor decreased as the anneal time increased. After a certain amount of annealing had been done, further processing had little effect. Based on these results, two anneal time-temperature cycles were selected for this work: 30 minutes at 380°C or 15 minutes at 440°C.

3.3 AC Conductivity and Dissipation Factor

The parallel conductance and capacitance of the MIM devices were measured from 100 Hz to 100 kHz. Figures 4 and 5 are plots of

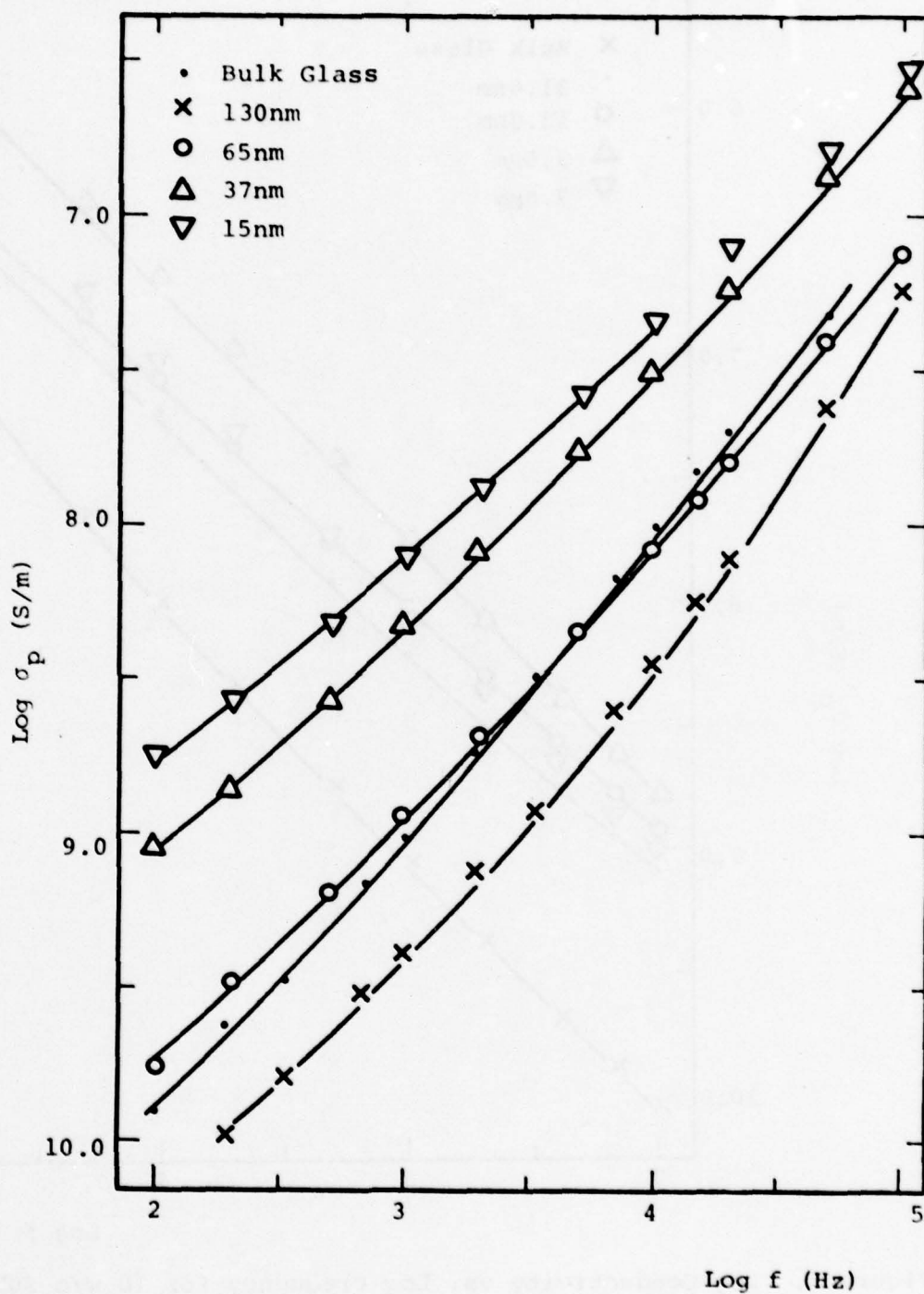


Figure 4. Log Conductivity vs. Log Frequency for Standard Glass Devices

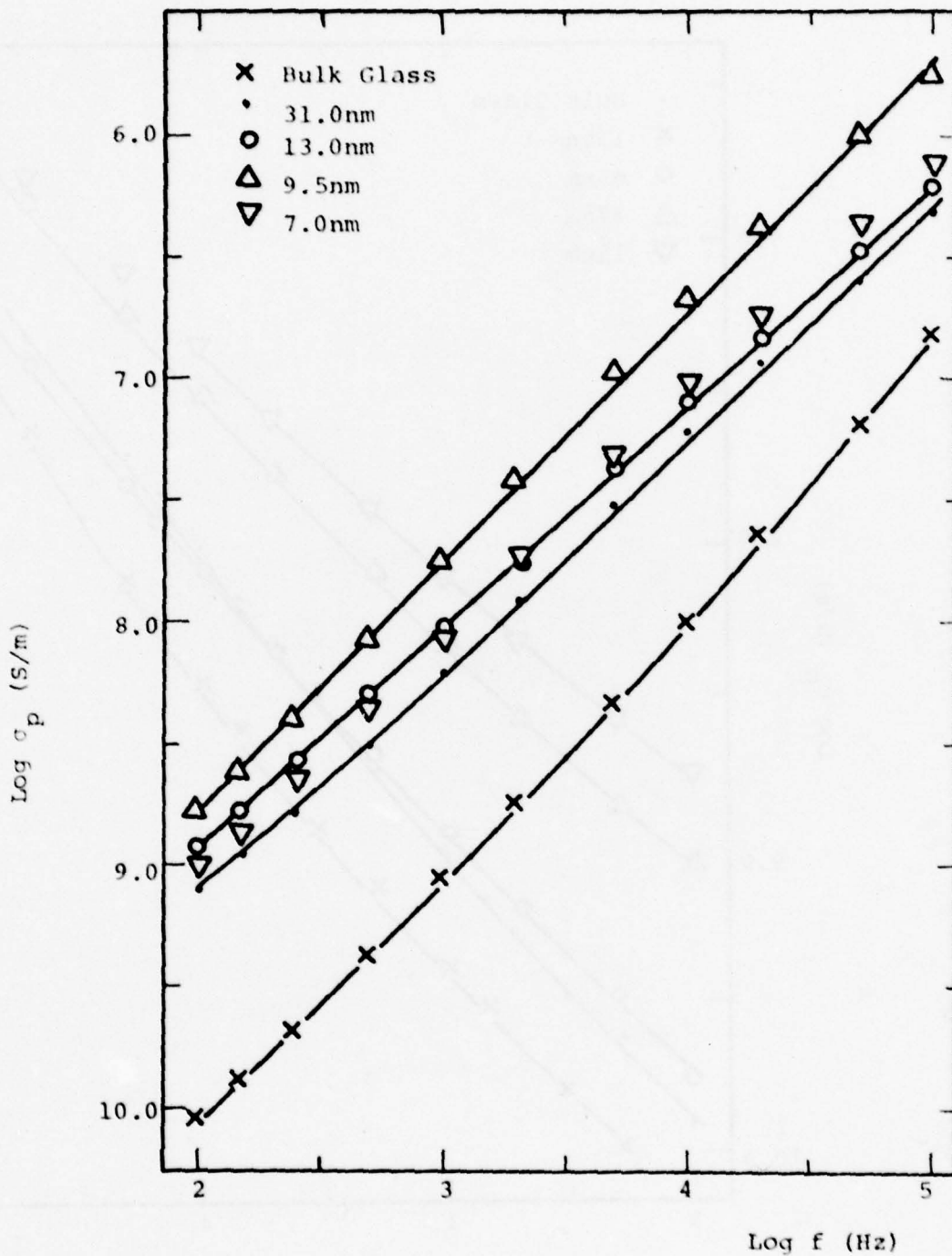


Figure 5. Log Conductivity vs. Log Frequency for 10 w/o Substrate Glass Devices

the parallel conductivities versus the log of the frequency for various thicknesses of the standard glass and 10 w/o substrate glass films respectively. The slope of each curve is approximately one. In general, the conductivity increases as the thickness decreases, with the only exceptions to this trend being the 7nm, 10 w/o substrate glass film and the standard bulk glass.

The three thinnest 10 w/o substrate glass samples were sputtered for 2 minutes, 1 minute, and 40 seconds, yielding calculated film thicknesses of 13.0, 9.5, and 7.0nm respectively. Because the conductivity of the film calculated to be 7.0nm thick was lower than that for the film calculated to be 9.5nm thick, it would have been desirable to make a direct measurement of film thickness; however, the films were too thin to get good interference patterns. It is, therefore, possible that the actual film thicknesses are different from those calculated. It is also possible that the change in conductivity could be caused by a change in the physical properties of the glass because compositional variations of the glass within the area of the electrodes becomes more probable for ultra-thin films.

The dissipation factor curves of Figures 6 and 7 for the standard and 10 w/o substrate glass devices reveal an increasing D as film thickness decreases. For the standard glass there is approximately a 1 1/2 order-of-magnitude difference between the bulk sample and the 15nm sputtered film. In addition, the bulk and 130nm samples had very similar characteristics, both displaying a broad minimum at ~ 2500 and ~ 6300 Hz respectively. The 65nm sample also appears to be approaching a minimum at a frequency just above 100K Hz,

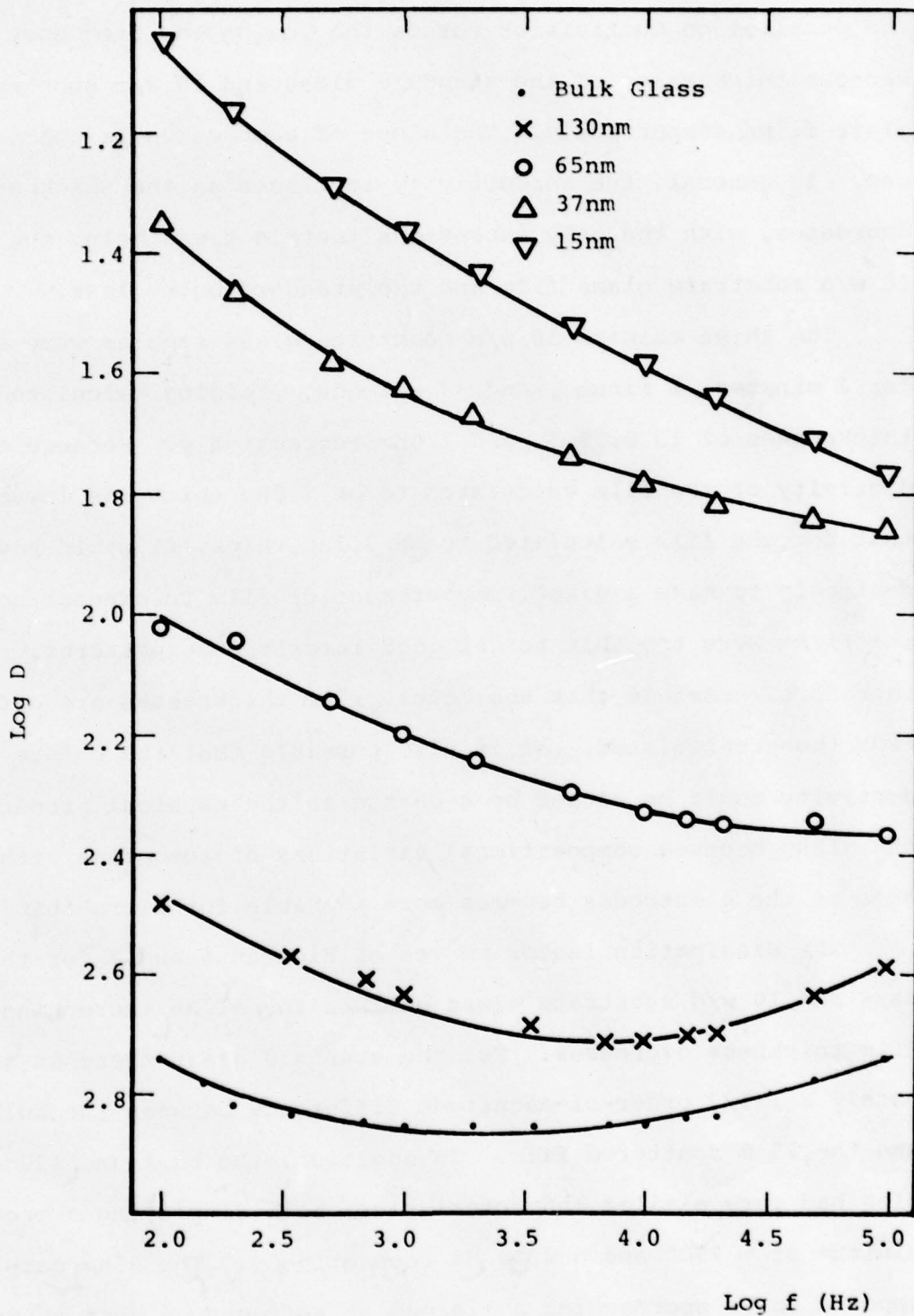


Figure 6. Dissipation Factor as a Function of Frequency and Film Thickness for Standard Glass Devices

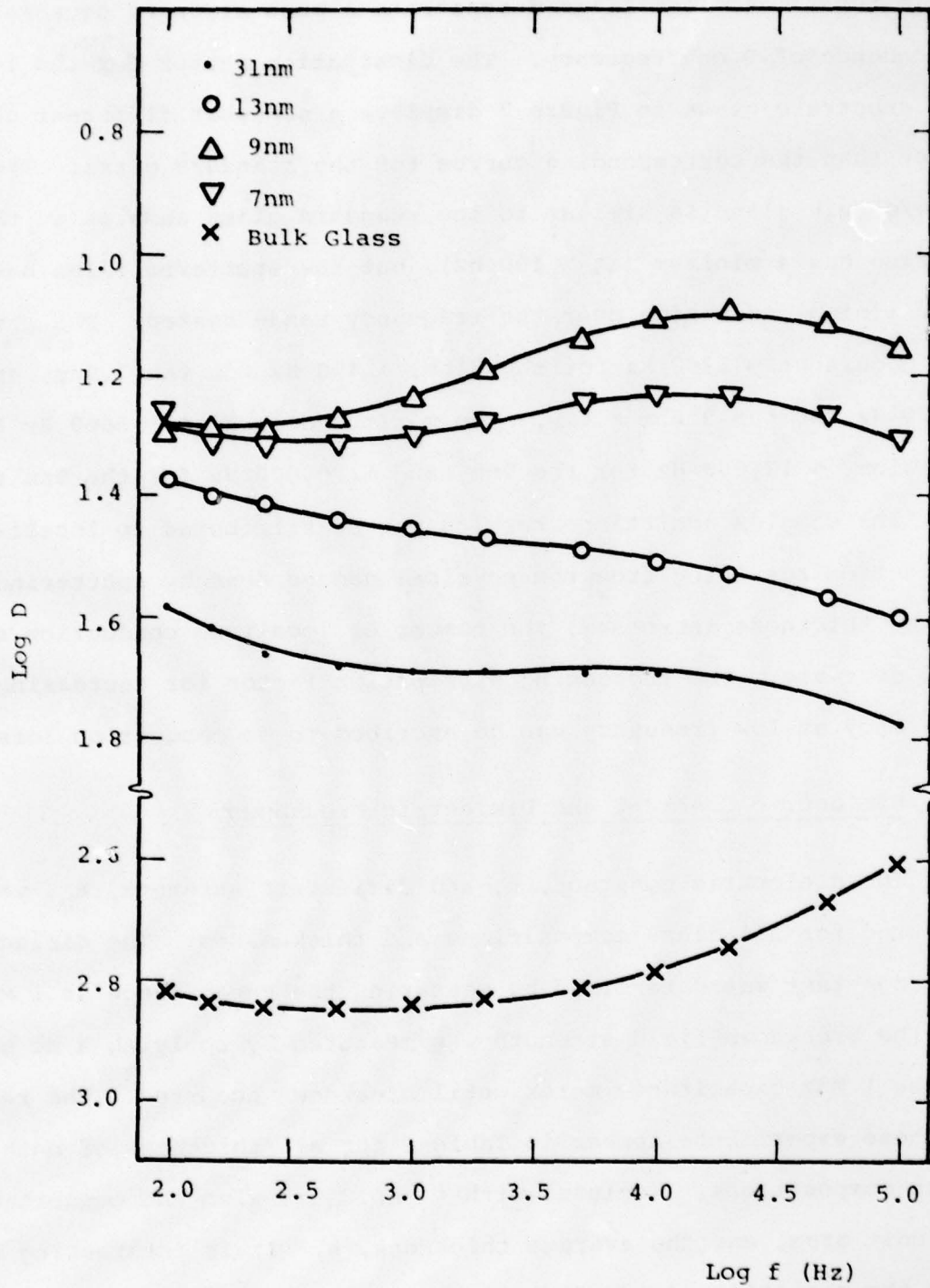


Figure 7. Dissipation Factor as a Function of Frequency and Film Thickness for 10 w/o Substrate Glass Devices

while the 37 and 15nm films demonstrate a much stronger decreasing dependence of D on frequency. The dissipation factor for the 10 w/o substrate glass in Figure 7 displays a somewhat different character than the corresponding curves for the standard glass. The 10 w/o bulk glass is similar to the standard glass samples in that it also has a minimum (at ~ 100 Hz), but the sputtered films have both minima and maxima over the frequency range tested. The minimum occurs at ~ 1200 Hz for the 31nm, ~ 400 Hz for the 7.0nm, and ~ 180 Hz for the 9.0nm films. The maximum occurs at ~ 5600 Hz for the 31nm, $\sim 12,600$ Hz for the 7nm, and $\sim 20,000$ Hz for the 9nm films.

The complex admittance results can be attributed to localized conduction resulting from the physical damage done by sputtering. As the thickness increases, the number of localized conduction sites will decrease. The increasing dissipation factor for decreasing frequency at low frequency can be ascribed to dc conduction losses.

3.4 Dielectric Constant and Dielectric Breakdown

The dielectric constant, k , and dielectric strength, E_b , were measured for all glass compositions and thicknesses. The dielectric constant was determined by measuring the capacitance at 1 MHz, and the breakdown field strength was measured by applying a dc bias to the 1 MHz capacitance meter until breakdown occurred. The results of these experiments appear in Table 2 for all thickness of both glass compositions. Included with k and E_b is also the capacitance per unit area, and the average thickness, s . It is interesting to note the variation of the dielectric constant with decreasing film

Table 2 Dielectric Constant and Dielectric Breakdown

Glass	s (nm)	C _p (μF/m ²)	k	E _b (V/m)
STD	130	233.	3.4	3.9 X 10 ⁸
	65	408	3.0	2.8 X 10 ⁸
	37	670	2.8	2.6 X 10 ⁸
	15	2300	3.9	2.5 X 10 ⁸
	10	3800	4.3	2.5 X 10 ⁸
	Bulk GL	.240	11.5	-----
10 w/o Subst.	31	1540	5.4	4.0 X 10 ⁸
	13	3030	4.4	5.1 X 10 ⁸
	9.5	4000	4.3	5.8 X 10 ⁸
	7.0	3180	2.5	5.7 X 10 ⁸
		Bulk GL	9.70	11.2

thickness; for the standard glass MIM's decreases from 3.4 to 2.8 and then increases to 4.3 while for the 10 w/o substrate glass, decreases monotonically from 5.4 to 2.5. This variation could be due to structural discontinuities in the glass. The dielectric strength remained essentially constant for each composition as the thickness varied, but the 10 w/o substrate glass breakdown field was over twice that of the standard glass for similar thicknesses. The fact that the bulk glass sample's dielectric constants of about 11 are twice the dielectric constants of the 10 w/o substrate glass MIMs and 4 times that of the standard glass MIMs could be due to thickness variations within the electrode areas of the MIMs.

3.5 DC Measurements

Samples were tested in a vacuum system specially built for temperature cycling. After mounting chips on the headers as described in Section 3.1, they were inserted in a brass collar which, in turn, was attached to a larger brass block which could be heated with a cartridge heater or cooled with liquid nitrogen. The device's top electrode was accessed by a spring-loaded probe mounted on an x-y-z motion micropositioner. The samples were biased by a battery operated power supply, and the device voltage (V) was measured with one electrometer and the current (I) with another. Both electrometers were battery operated. The dc analysis consisted of two basic experiments; measuring current as a function of voltage at a constant temperature, and measuring current as a function of temperature at constant voltage. The dc experiments were performed on both the 10 w/o substrate glass and the standard glass devices.

However, because of breakdown problems associated with the standard glass, good, reproducible data could not be obtained for this dielectric at temperatures other than room temperature. Three dielectric thicknesses of the 10 w/o substrate glass were sufficiently thin to get measurable currents and reproducible data over several orders of magnitude of current and voltage.

In general, it was determined that the log of current was dependent on the square root of voltage and inversely proportional to temperature. This was observed independent of film thickness, electrode metal (Au and Al), temperature, direction of the field, or glass composition (for both standard and 10 w/o substrate glass). Figures 8-10 are plots of the log of current density versus the square root of voltage at room temperature across a standard glass film 15 nm thick (Figure 8), a 10 w/o substrate glass film 13.0nm thick (Figure 9), and a 10 w/o substrate glass film (Figure 10) with Al as the top metal (all electrodes are gold unless otherwise noted). Each curve has a remarkably similar characteristic; they are linear for almost 4 orders of magnitude in current, and there is no perceptible change in reversing polarity. As later results will show, the slope is dependent on film thickness, temperature, and voltage. The other interesting behavior associated with these results is the low field characteristic, where the current decreases rapidly with voltage. It was observed in all thicknesses tested for both glass compositions. Reversing polarity had no effect, nor did changing the top electrode metal. Even though a different threshold was observed for gold and aluminum electrodes, differences in threshold as large as this were observed for the same metal from sample-to-sample.

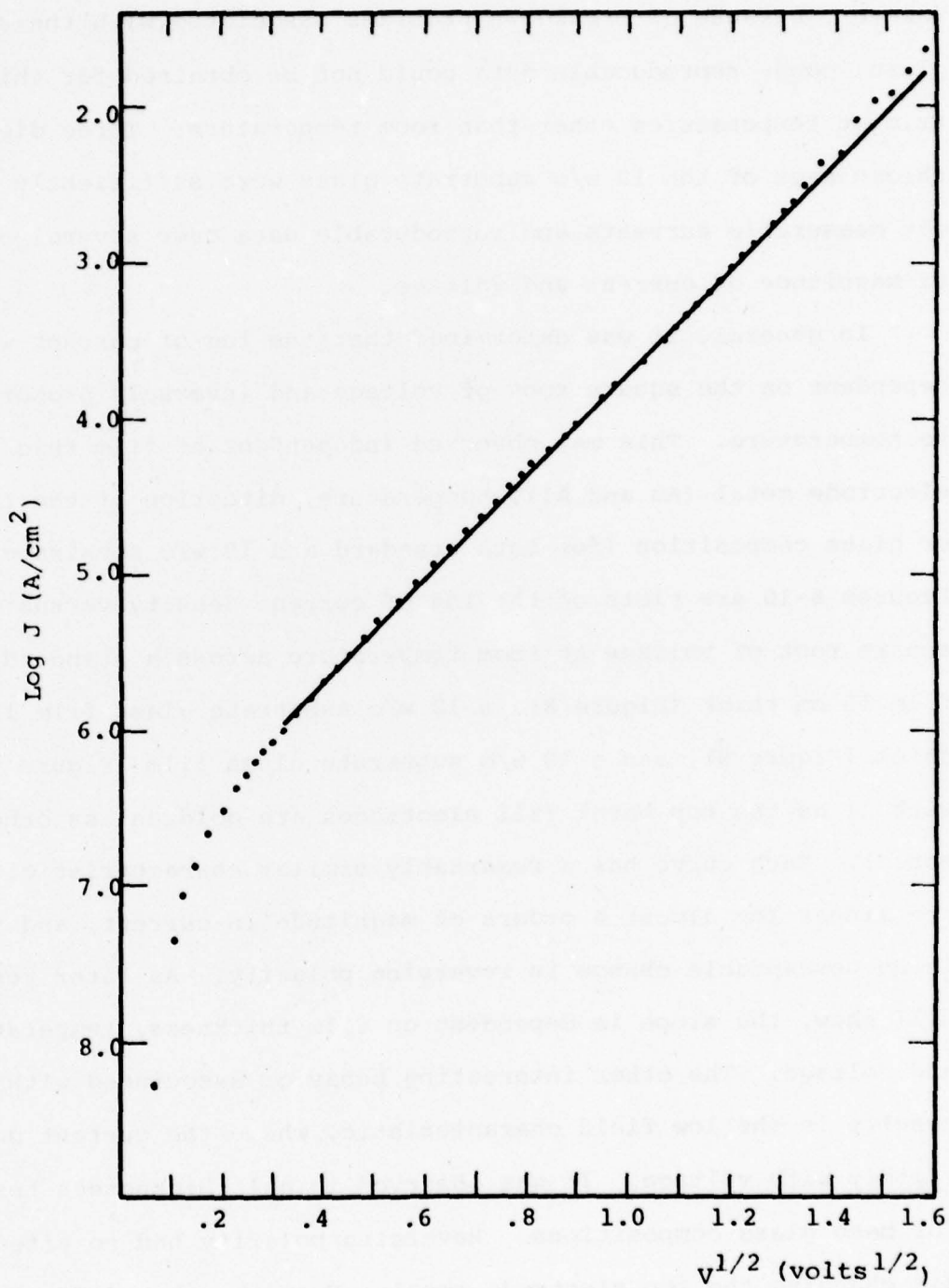


Figure 8. Current Density-Voltage Dependence of a 15nm Standard Glass MIM at 25°C

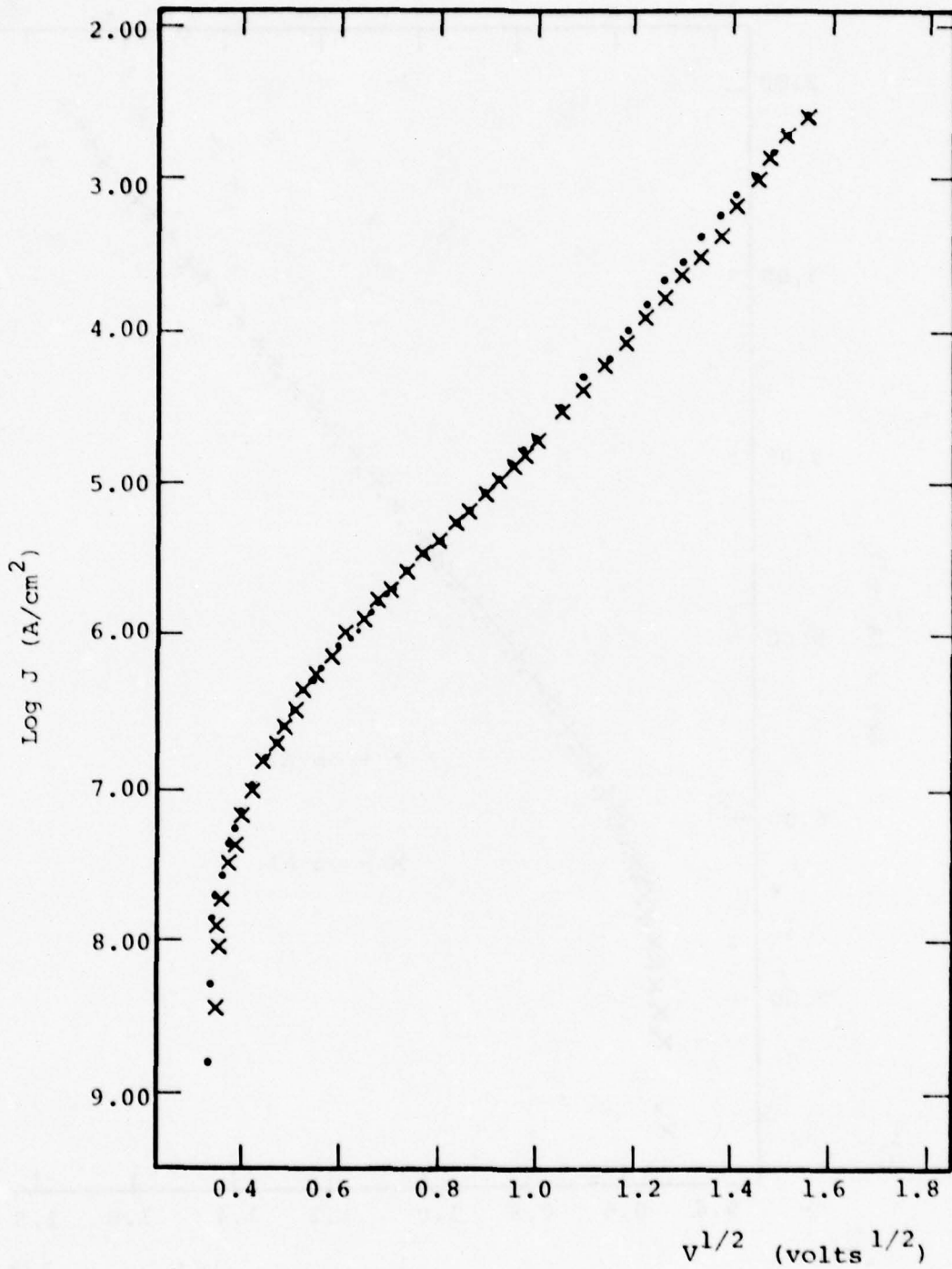


Figure 9. Current Density-Voltage Dependence of a 13nm 10 w/o Substrate Glass MIM at 25°C

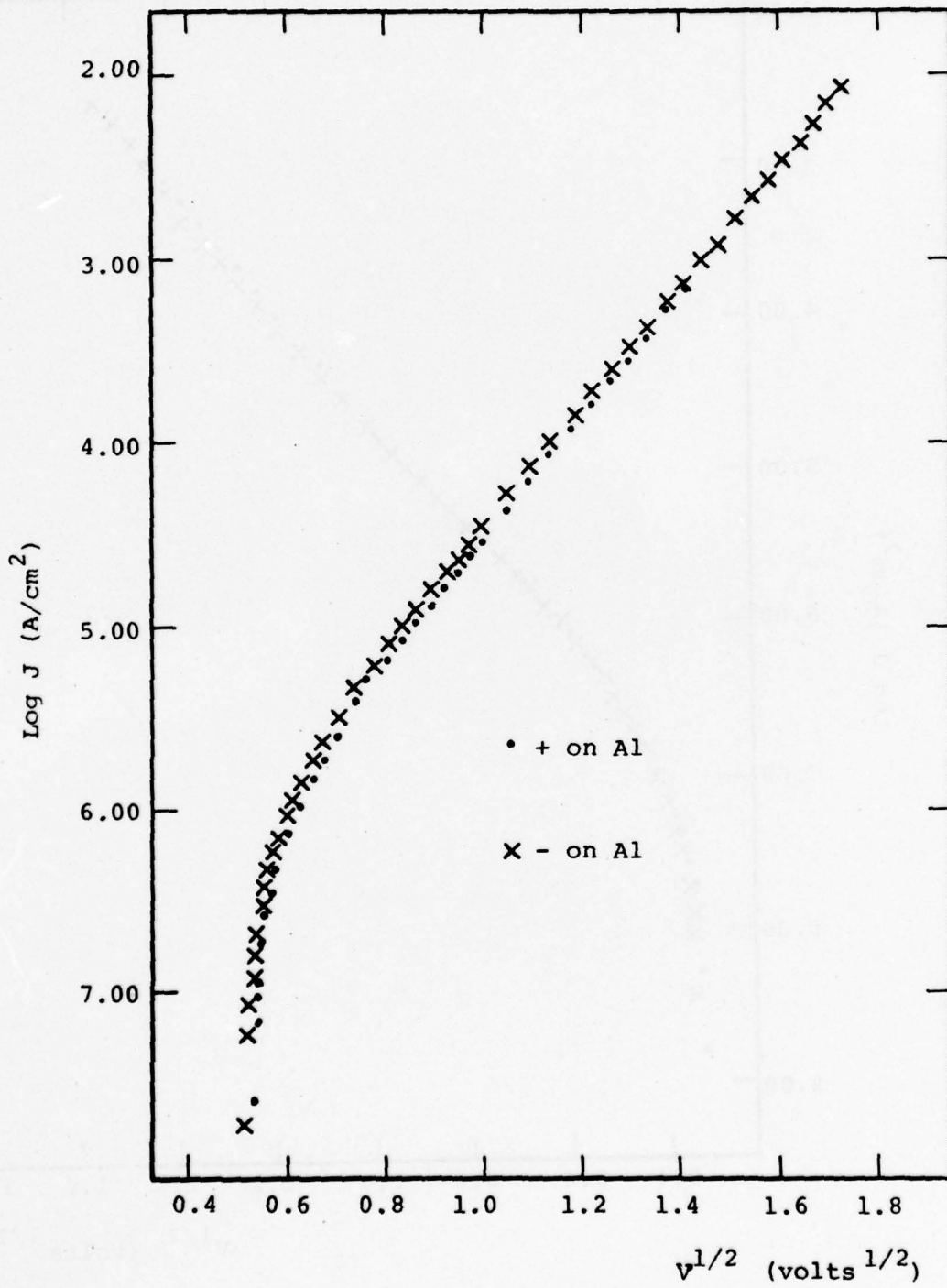


Figure 10. Current Density-Voltage Dependence of a 10 w/o Substrate Glass MIM with an Aluminum Top Electrode at 25°C

Annealing raised the dc current density of the film for a given voltage and in-so-doing improved the device stability. It is believed this was due to improving the interface between the top gold electrode and the glass. Figure 11 is a plot of the standard glass film current-voltage characteristic before and after the anneal. The anneal has shifted the curve up by two orders-of-magnitude. The low voltage slope has not changed appreciably, but the steeper sloped region is no longer visible. Two 10.0nm standard glass devices that were annealed at 380°C for 10 minutes showed the same shape and position of the threshold voltage, but the magnitude of the current was different by 4 orders-of-magnitude (see Figure 12). The slopes of the lines in Figure 12 are almost identical to each other, but they are lower than the slope of the 15.0nm films (Figure 11) by about a factor of two. The lower conductivity sample was cooled down to -37°C, and the temperature was slowly decreased from that point. The x's on Figure 12 represent points taken as the sample was cooled down to -60°C, and these datum points are coincident with the room temperature values, which suggests a temperature independent transport mechanism.

The 10 w/o substrate glass devices were much more stable than the standard glass devices under thermal cycling. The current-voltage data for a 10 w/o substrate glass device that was 13.0nm thick plot as straight lines (Figure 13) with a higher slope at -2.5°C than at room temperature. The log of the current densities versus reciprocal temperature plot as straight lines at all field strengths (Figure 14), each with a successively lower slope for increasing V. Similar results were obtained for a 9.5nm, 10 w/o

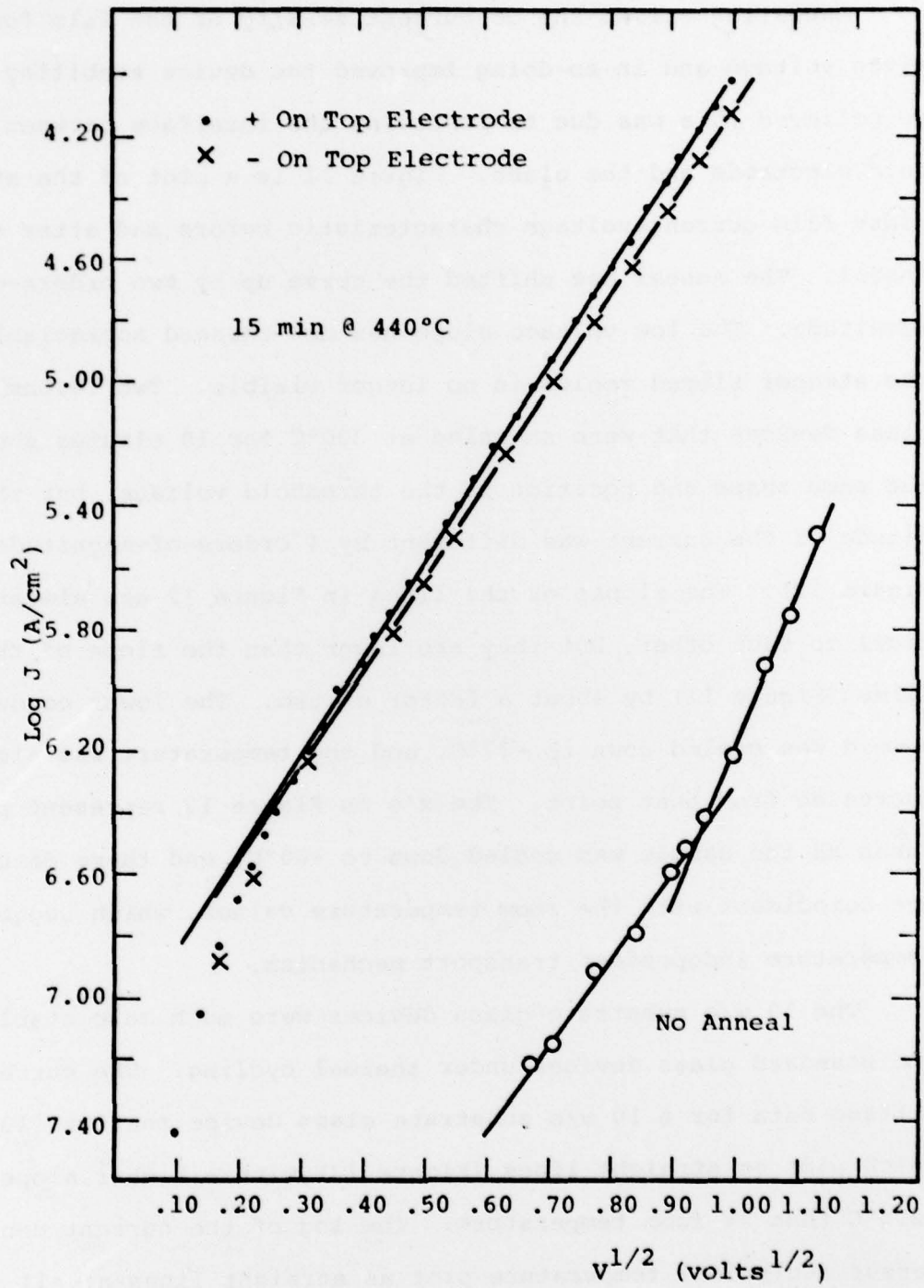


Figure 11. Current Density-Voltage Dependence of a 15nm Standard Glass MIM Before and After Annealing

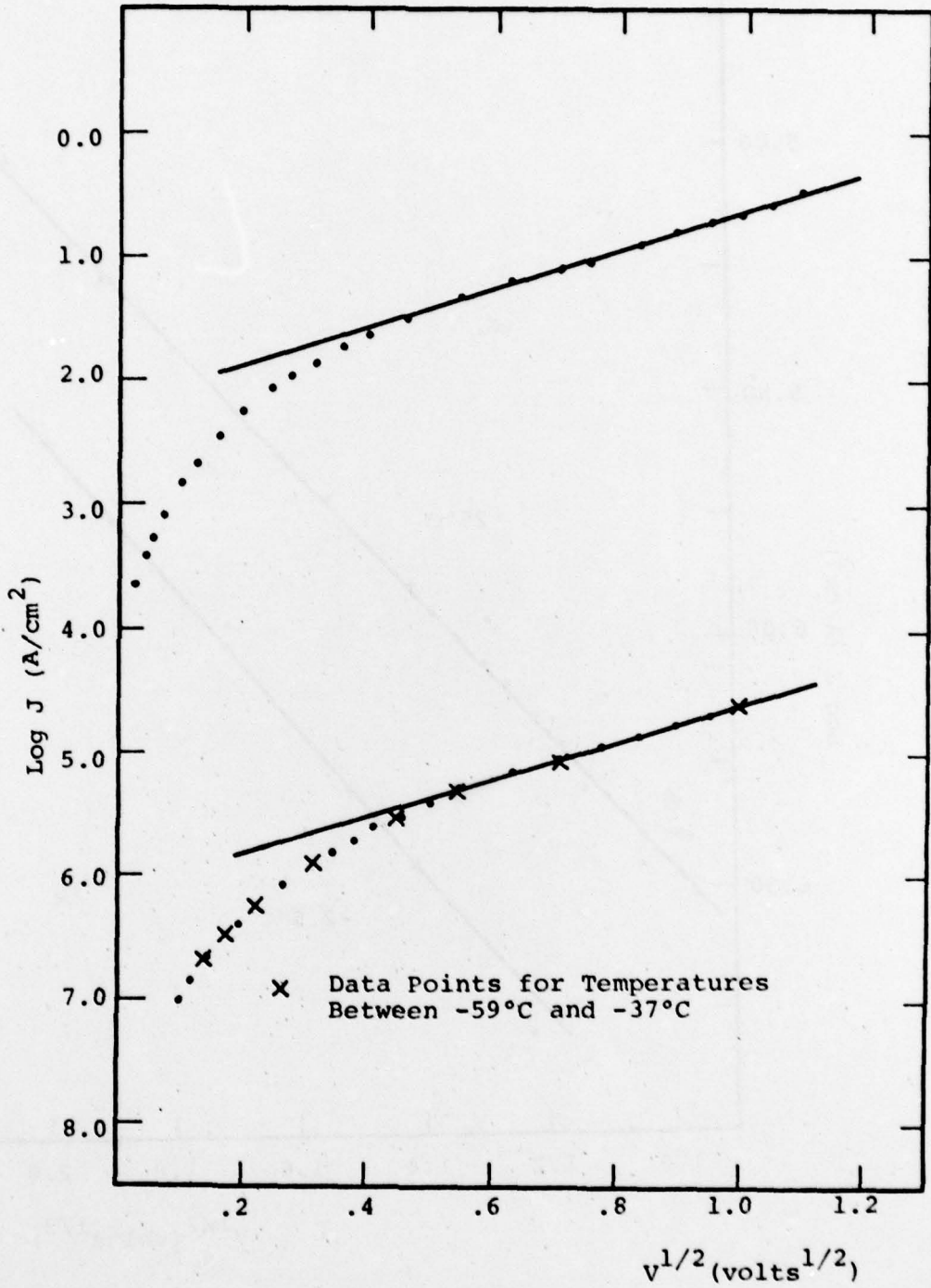


Figure 12. Current Density-Voltage Dependence of Two 10nm Standard Glass MIMs

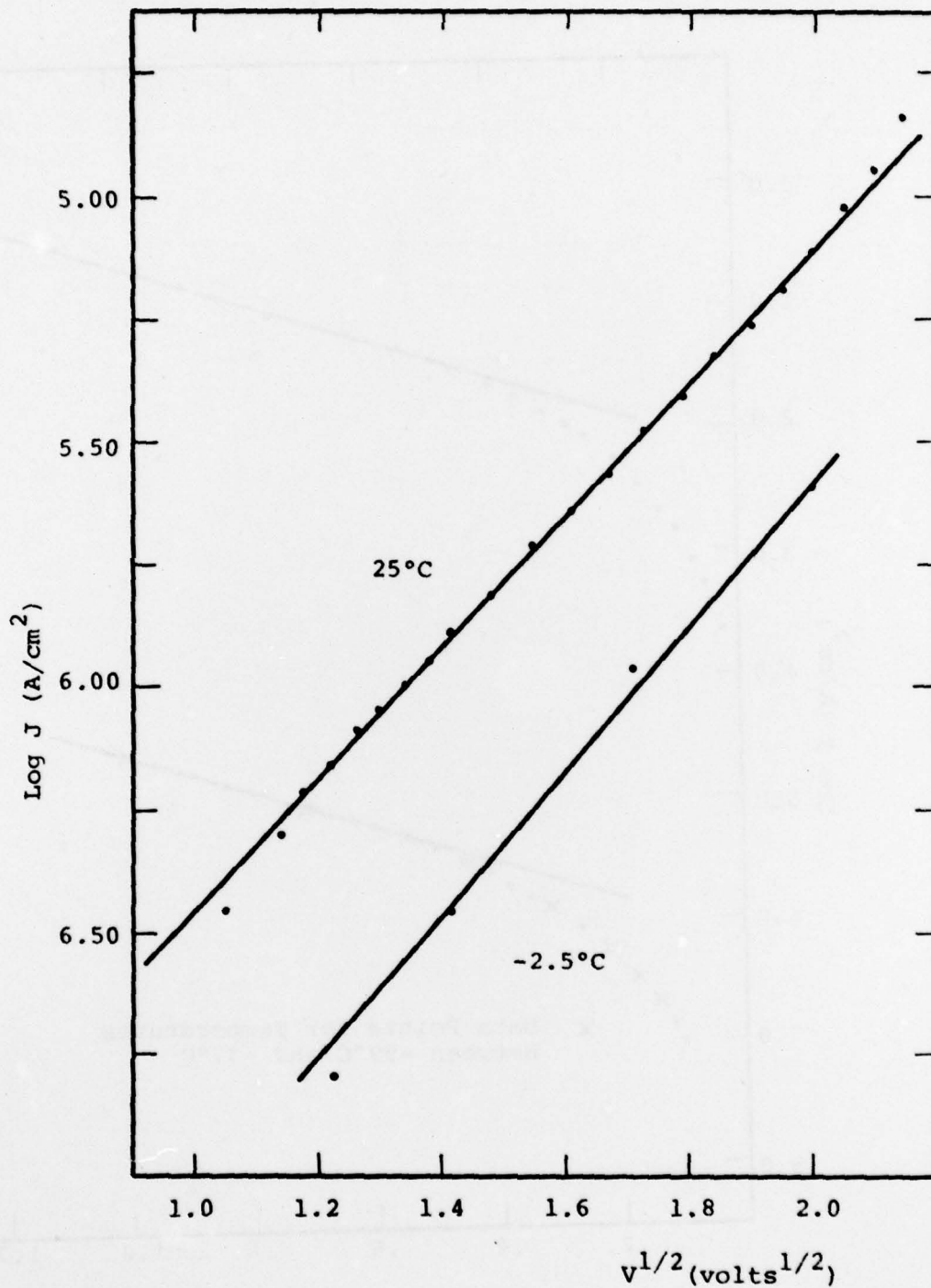


Figure 13. Current Density-Voltage Dependence of a 13nm 10 w/o Substrate Glass MIM at Two Temperatures

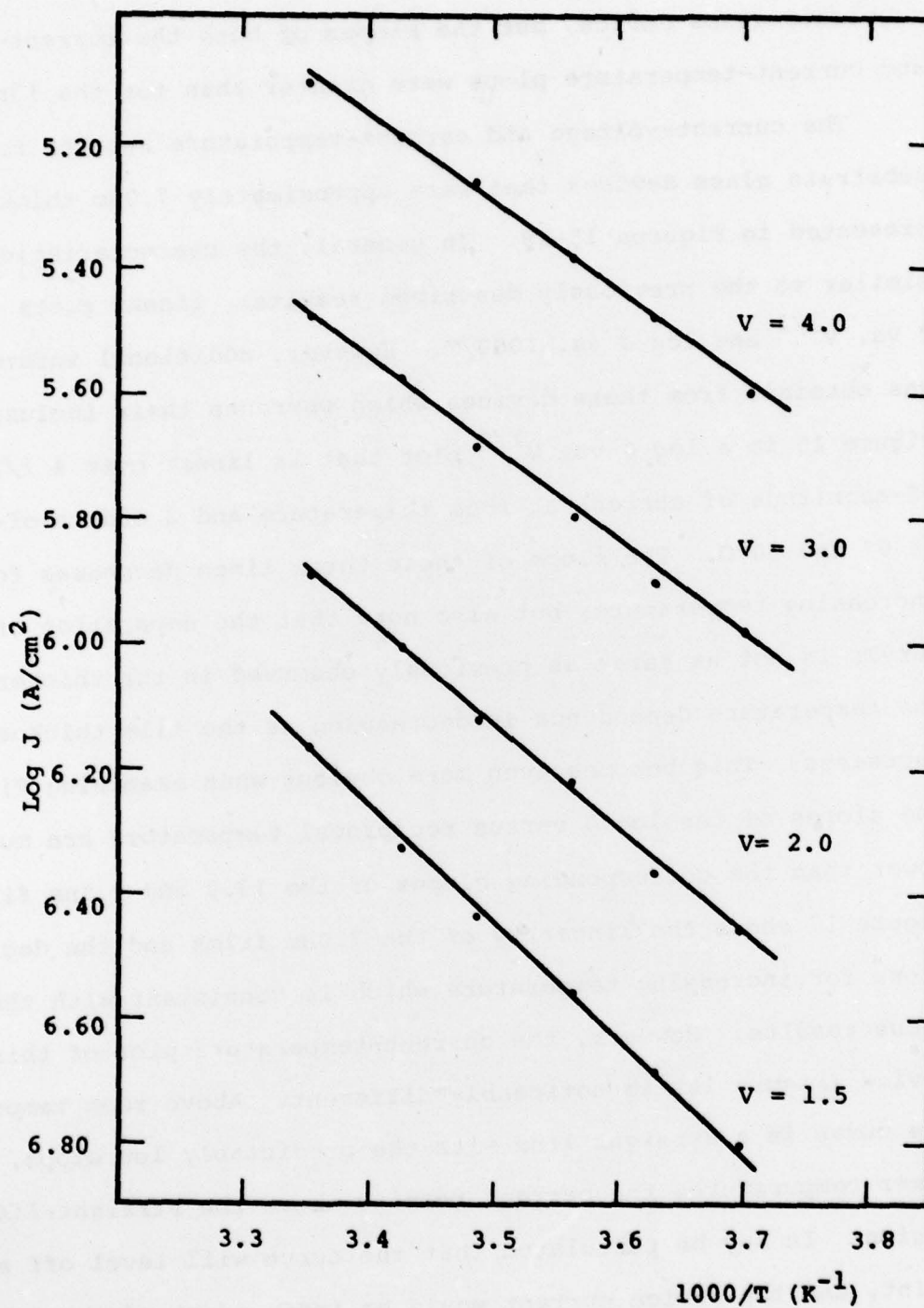


Figure 14. Current Density-Temperature Dependence of a 13nm 10 w/o Substrate Glass MIM at Four Voltages

substrate glass device, but the slopes of both the current-voltage and current-temperature plots were greater than for the 13nm device.

The current-voltage and current-temperature results for 10 w/o substrate glass devices that were approximately 7.0nm thick are presented in Figures 15-18. In general, the characteristics are similar to the previously described results: linear plots of $\log J$ vs. $V^{1/2}$ and $\log J$ vs. $1000/T$. However, additional information was obtained from these devices which warrants their inclusion. Figure 15 is a $\log J$ vs. $V^{1/2}$ plot that is linear over 4 1/2 orders-of-magnitude of current at room temperature and 3 orders-of-magnitude at 0° and 50°C. The slope of these three lines decreases for increasing temperature, but also note that the separation of the curves is not as large as previously observed in the thicker films. The temperature dependence is decreasing as the film thickness decreases. This becomes even more obvious when examining Figure 16. The slopes of the $\log J$ versus reciprocal temperature are much lower than the corresponding slopes of the 13.0 and 9.5nm films. Figure 17 shows the linearity of the 7.0nm films and the decreasing slope for increasing temperature which is consistent with the previous results. However, the current-temperature plot of this device (Figure 18) is noticeably different. Above room temperature the curve is a straight line with the predictably low slope, but at lower temperatures the current remains above the straight-line region. It may be postulated that the curve will level off at some point, and the device current would be independent of the temperature. For the given thickness and applied field, this would indicate a tunneling mechanism for charge transport.

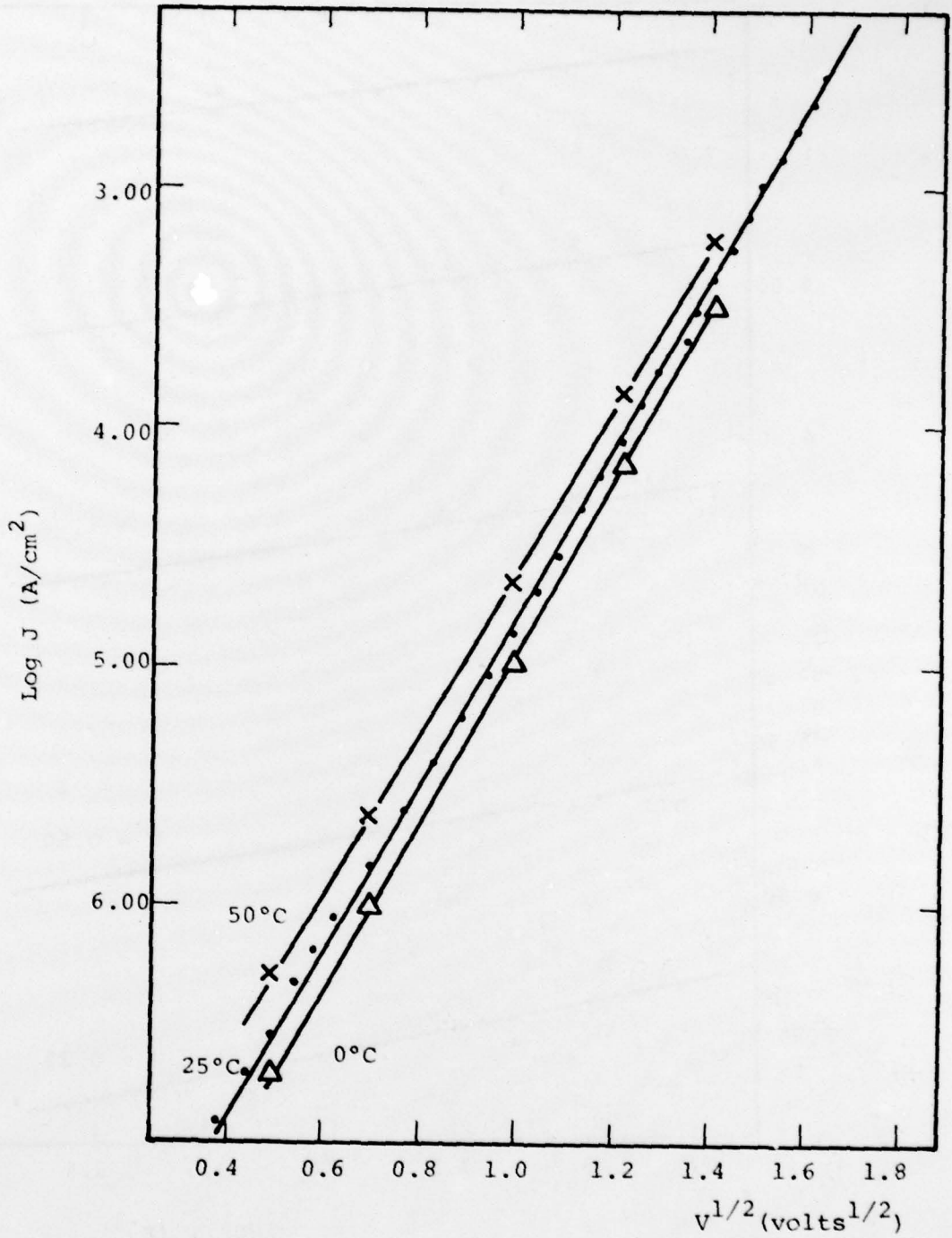


Figure 15. Current Density-Voltage Dependence for a 7nm 10 w/o Substrate Glass MIM at Three Temperatures

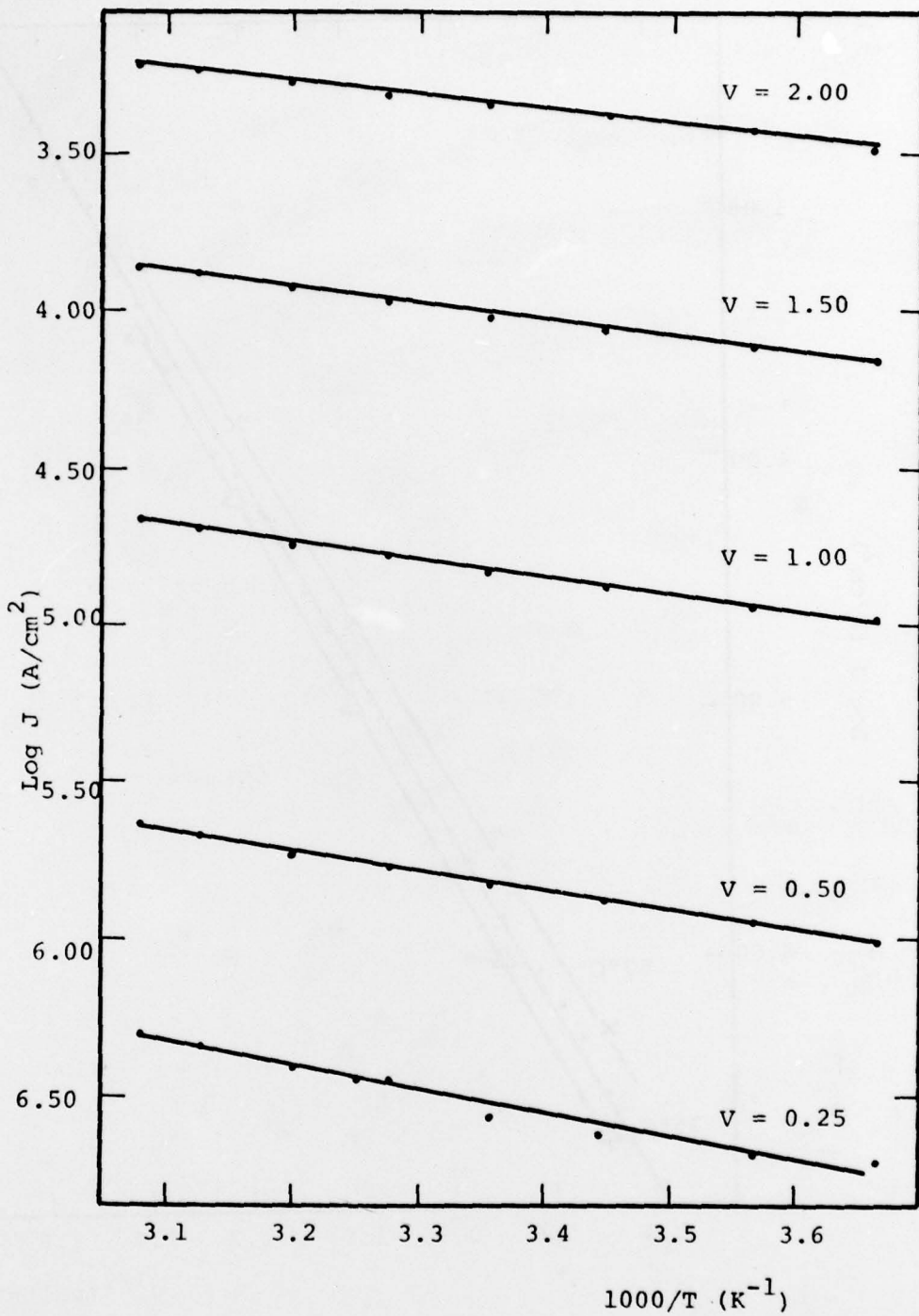


Figure 16. Current Density-Temperature Dependence for a 7nm 10 w/o Substrate Glass MIM at Five Voltages

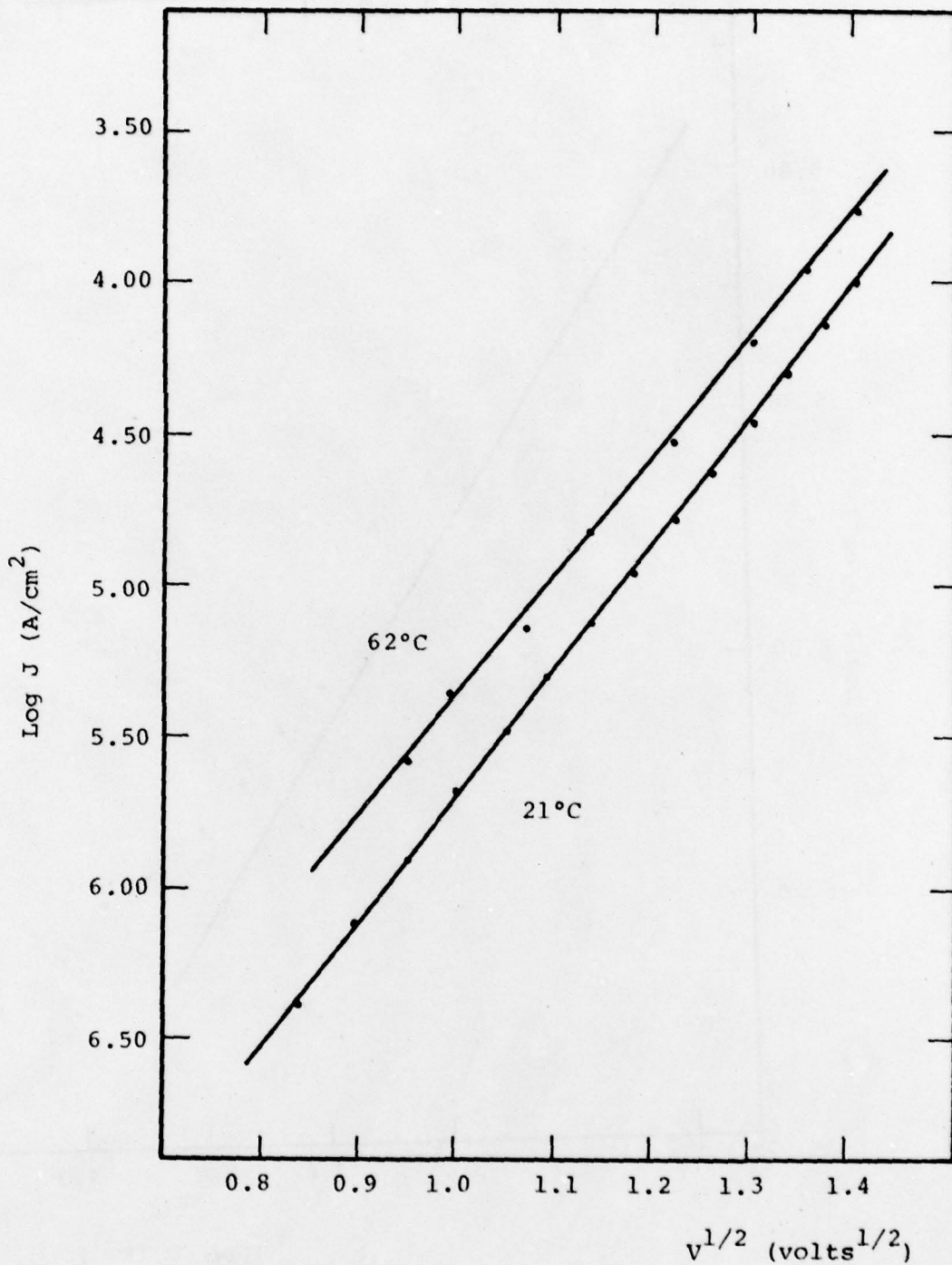


Figure 17. Current Density-Voltage Dependence for a 7nm ITO w/o Substrate Glass MIM at Two Temperatures

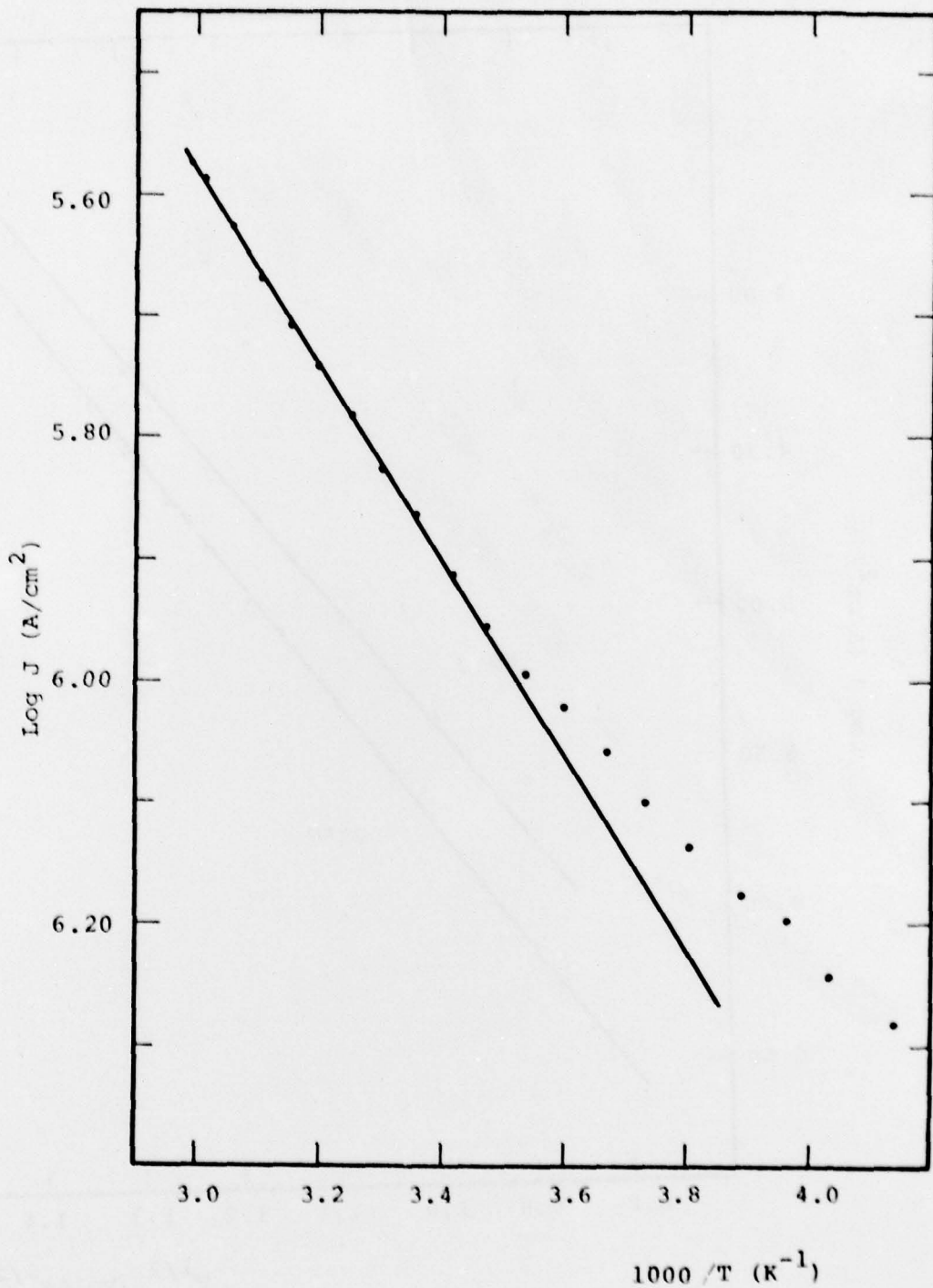


Figure 18. Current Density-Temperature Dependence for a 7nm 10 w/o Substrate Glass MIM at 0.5 Volt

The results of the current-voltage and current-temperature measurements have consistently demonstrated that the log of device current is dependent on the square root of voltage and inversely proportional to temperature, and that the voltage dependence is much stronger than the temperature dependence. The straight-line plots of the log of the current density versus the square root of the voltage over several orders-of-magnitude of current emphatically suggest a Schottky emission or Frenkel-Poole emission mechanism. One way to separate the two mechanisms is to calculate the dielectric constant (k) using the slope from the $\log J$ vs. $V^{1/2}$ plots with the sample thickness (s) and temperature. The current density for each mechanism is given by

$$J_S \propto T^2 \exp\{q[(qV/4\pi\epsilon_0 ks)^{1/2} - \phi_s]/kT\} \quad (1)$$

$$J_{F-P} \propto (V/s) \exp\{q[(qV/\pi\epsilon_0 ks)^{1/2} - \phi_{F-P}]/kT\} \quad (2)$$

where q is the electronic charge, ϵ_0 the permittivity of free space, ϕ_s the Schottky barrier height, and ϕ_{F-P} the Frenkel-Poole trap well depth both in volts, and k is Boltzmann's constant.

In graphing $\log J$ vs. $V^{1/2}$, the slope m_V of the linear portion corresponds to

$$2.3 m_V = \frac{q}{kT} \left(\frac{q}{4\pi\epsilon_0 ks} \right)^{1/2} \quad \text{Schottky} \quad (3)$$

$$2.3 m_V = \frac{q}{kT} \left(\frac{q}{\pi\epsilon_0 ks} \right)^{1/2} \quad \text{Frenkel-Poole} \quad (4)$$

For any given thickness, temperature, and corresponding slope, the dielectric constant can be calculated from:

$$\begin{aligned} k &= (q \sqrt{3/4\pi\epsilon_0 k^2}) (1/s(2.3 m_V T)^2) \\ &= 0.03645/(s(m_V T)^2) \end{aligned} \quad \text{Schottky (5)}$$

or

$$\begin{aligned} k &= (q \sqrt{3/\pi\epsilon_0 k^2}) (1/s(2.3 m_V T)^2) \\ &= 0.1458/(s(m_V T)^2) \end{aligned} \quad \text{Frenkel-Poole (6)}$$

A dielectric constant was calculated for each data set for each mechanism; for the Frenkel-Poole case the average k was 18 with a standard deviation of 18 percent, and for the Schottky case the average k was 4.5 with a standard deviation of 18 percent. Based on a comparison of these results with the measured dielectric constants (Table 2) the more likely mechanism for conduction through the glass films is Schottky emission.

To calculate ϕ_s , the Schottky barrier height, the slopes ($m_{1/T}$) of the log J vs. $1000/T$ data were used along with Eq. 1 to yield:

$$\begin{aligned} \phi_s &= (qV/4\pi\epsilon_0 ks)^{1/2} - \frac{(2.3 \times 10^3) m_{1/T} k}{q} \\ &= 1.20(10^{-5}) (V/s)^{1/2} - 0.199 m_{1/T} \end{aligned} \quad (7)$$

Averaging the values of ϕ_s calculated from Eq. 7 for each data set gave a barrier height of 0.38 volts, which is quite consistent with barrier heights reported for Schottky emission.

4. FUTURE WORK

The kinetics of the initial stage of liquid phase sintering of RuO_2 will be calculated from the ripening data and the solubility data. These results will then be correlated utilizing the previously developed models for microstructure development, and the influence of glass composition established. The effects of substrate dissolution on charge transport processes in nonsintered contacts will be modeled, and the dependence of both the glass properties and the electrical properties of the nonsintered contacts on glass composition will be incorporated into a revised charge transport model for thick film resistors.

5. REFERENCES

1. R. W. Vest, "The Effects of Substrate Composition on Thick Film Circuit Reliability," Final Technical Report on Contract No. N0019-76-C-0354, 28 February 1977.
2. R. W. Vest, "The Effects of Substrate Composition on Thick Film Circuit Reliability," Final Technical Report on Contract No. N0019-77-C-0327, 28 February 1978.
3. R. W. Vest, "The Effects of Substrate Composition on Thick Film Circuit Reliability," Final Technical Report on Contract No. N0019-78-C-0236, 28 February 1979.
4. R. W. Vest, "The Effects of Substrate Composition on Thick Film Circuit Reliability," Quarterly Report No. 1 on Contract No. N0019-79-C-0240, 1 May 1979.
5. G. S. Fulcher, "Analysis of Recent Measurements of the Viscosity of Glasses," J. Am. Ceram. Soc., 8 (6), 339-55-(1925).

6. STATEMENT OF ESTIMATED COSTS

Contract No. N0019-79-C-0240

February 1, 1979 - January 31, 1980

Beginning Fund Balance	\$ 40,000.00
Funds Expended Through 7/31/79	<u>19,394.42</u>
Funds Remaining	\$ 20,605.58

Planned Expenditures (Approximate)

August	\$3425
September	3425
October	3425
November	3425
December	3425
January	3480